2016

Porphyrin-modified antimicrobial peptide indicators for detection of bacteria

Brandy J. Johnson
Naval Research Laboratory, brandy.white@nrl.navy.mil

Chris R. Taitt
Naval Research Laboratory

Apre Gleaves
Howard University

Stella H. North
Naval Research Laboratory

Anthony P. Malanoski
Naval Research Laboratory

See next page for additional authors

Sensing and Bio-Sensing Research 8 (2016) 1–7

Contents lists available at ScienceDirect

Sensing and Bio-Sensing Research

journal homepage: www.elsevier.com/locate/sbsr

Porphyrin-modified antimicrobial peptide indicators for detection of bacteria

Brandy J. Johnson [a,*], Chris R. Taitt [a], Apre Gleaves [b,1], Stella H. North [a,2], Anthony P. Malanoski [a], Iwona A. Leska [c], Edikan Archibong [d,3], Stormie M. Monk [e,4]

[a] Center for Bio/Molecular Science & Engineering, Naval Research Laboratory, Washington, DC 20375-5348, USA
[b] Chemistry Department, Howard University, Washington, DC 20059, USA
[c] NOVA Research Incorporated, Alexandria, VA 22308, USA
[d] Department of Chemical and Biomedical Engineering, University of South Florida, Tampa, FL 33620, USA
[e] Fayetteville State University, Fayetteville, NC 28301, USA

ARTICLE INFO

Article history:
Received 9 December 2015
Accepted 14 February 2016
Available online xxxx

Keywords:
Antimicrobial peptide
Porphyrin
Bacterial detection
Absorbance
Fluorescence

ABSTRACT

This study demonstrates the potential of porphyrin modified antimicrobial peptides for indication of bacterial targets on the basis of changes in the spectrophotometric characteristics of the construct. Detection is a result of changes in the structure of the antimicrobial peptide upon target binding. Those constructs comprised of peptides that offer little or no change in conformation upon interaction with bacterial cells demonstrated negligible changes in absorbance and fluorescence when challenged using *Escherichia coli* or *Bacillus cereus*. CD analysis confirms the presence/absence of conformational changes in the porphyrin-peptide constructs. Differing spectrophotometric responses were observed for constructs utilizing different peptides. The incorporation of metals into the porphyrin component of the constructs was shown to alter their spectrophotometric characteristics as well as the resulting absorbance and fluorescence changes noted upon interaction with a target. The described constructs offer the potential to enable a new type of biosensing approach in which the porphyrin-peptide indicators offer both target recognition and optical transduction, requiring no additional reagents.

1. Introduction

Antimicrobial peptides (AMPs) are a group of biomolecules that have evolved to recognize and kill target microbes by binding to and disrupting cell membranes. Several unique characteristics of AMPs make them attractive alternatives to antibodies for detection of microbial biothreats: resistance to proteases; stability to environmental extremes; and high affinity, overlapping (but not identical) binding interactions with microbial membranes and membrane components. Arrays of AMPs have been used to detect and classify microbial pathogens with similar sensitivity to antibody-based assays; their broad-spectrum binding activities also provide the potential for detection of unknown microbes [11,12,16,18,27]. In previous studies, surface-immobilized AMPs mediated target binding, and an additional "tracer" (e.g., labeled antibody or non-specific dye) was required for signal transduction. This constraint increases the number of reagents required and the overall complexity of the assay. Development of an AMP-based material that is capable of both target recognition and signal generation without addition reagents or processing steps is highly desirable. This type of construct would provide greatly enhanced potential for application of AMP-based detection techniques in autonomous and distributed sensing platforms.

A number of publications report use of porphyrin-peptide conjugates for targeting and photodestruction of cells [3–5,7,10,13,24]. In these studies, the antimicrobial peptide domain is used to interact with the appropriate cell (cancer cell, Gram-negative bacterial pathogen), while the porphyrin moiety is used as a source of reactive oxygen species upon illumination [21]. Porphyrins are large macrocyclic compounds with strong absorbance and fluorescence characteristics. They have been applied in a wide variety of detection approaches due to the sensitivity of those characteristics to their immediate environment. Spectrophotometric and binding characteristics can be altered through modification of the porphyrin structure. Several reports have described modifications using single amino acids or dipeptides [2,29,33]. Binding of proteins by these porphyrin derivatives resulted in changes to their fluorescence characteristics, and arrays of the constructs were applied to discrimination of proteins. Modification of the periphery of a porphyrin using cytosine was similarly applied to detection of guanine [6]. Other works have shown that porphyrins can be used to report

* Corresponding author.
E-mail address: brandy.white@nrl.navy.mil (B.J. Johnson).
[1] At NRL Summer 2013/2014 through NSF/ONR internship.
[2] Current Address: Currently Latham & Watkins LLP, Washington, DC 20004.
[3] At NRL Summer 2013 through ASEE internship.
[4] At NRL Summer 2012 through ASEE internship.

http://dx.doi.org/10.1016/j.sbsr.2016.02.005

conformational changes in enzymes upon substrate binding when the porphyrin-enzyme interaction results in competitive or mixed-type enzymatic inhibition [30,31].

This study sought to demonstrate the potential for antimicrobial peptides modified using porphyrins in indication of the presence of bacterial cells. The goal was development of constructs providing an avenue for achieving reagentless detection and classification of bacterial targets. Sensing in this case would utilize changes in the local environment of a covalently attached porphyrin resulting from conformational changes in the antimicrobial peptide. While others have proposed application of porphyrin-peptide conjugates as imaging agents (e.g., [13]), this approach would provide the potential for use of an array of peptide-porphyrin conjugates in detection of bacteria with broad classification of the detected cells based on the differential changes in the spectrophotometric characteristics of the porphyrin-peptide conjugates. Here, synthesis and characterization of a set of four porphyrin-AMP constructs is presented. Their utility with regard to the potential for indication of bacterial targets is discussed.

2. Methods

5-Mono(4-carboxyphenyl)-10, 15, 20-triphenyl porphine (C_1TPP) was obtained from Frontier Scientific (Logan, UT). Vanadium (III) bromide, zinc chloride, cobalt (II) chloride, and dimethylsufloxide (DMSO) were obtained from Sigma-Aldrich (St. Louis, MO). 1-Ethyl-3-(3-dimethylaminopropyl) carbodiimide hydrochloride (EDC), N-hydroxysuccinimidyl ester (NHS) and sulfo-NHS were purchased from Pierce Thermo Scientific (Rockland, IL). Antimicrobial peptides indolicidin (Ind), bactenecin (Bac), and cecropin A (1–8)-melittin (1–18) hybrid peptide (CeMe) were purchased from American Peptide Company (Sunnyvale, CA); polymyxin E (PME) was obtained from Sigma-Aldrich. Sequences are provided in Table 1.

Direct covalent attachment of C_1TPP to the above peptides was accomplished under anhydrous conditions with carbodiimide-mediated coupling. Stock solutions of C_1TPP, EDC, NHS, bactenecin, and indolicidin were prepared in absolute ethanol prior to mixing; as neither PME nor CeMe is highly soluble in absolute ethanol, stock solutions of these peptides were prepared in 4:1 (*v*/v) ethanol:acetonitrile. The composition of the reaction mixtures (molar equivalents) were as follows: 1 peptide: 1.1 C_1TPP: 1.2 EDC: 1 NHS. After completion of the coupling reaction (≫2 h), reaction mixtures were diluted with water and dialyzed (1000 molecular weight cutoff) exhaustively against water and phosphate-buffered saline (PBS). Construct concentrations are estimated based on the initial concentration of AMP and the total final volume of the preparation. Metal variants were prepared through incubation of porphyrin-AMP constructs (25 μM) with metal salts (vanadium (III) bromide; zinc chloride; cobalt (II) chloride; 50 μM) in aqueous solution [8]. The solutions were thoroughly mixed and heated to 60 °C for 3 h before storage at 4 °C for at least 48 h. Metal incorporation was evaluated based on changes in absorbance and fluorescence characteristics. Construct names are abbreviated to indicate the metal, porphyrin, and AMP used; for example, CoC_1-Ind is the cobalt variant of C_1TPP conjugated to the indolicidin peptide.

The bacterial targets for binding studies, *Escherichia coli* (XL1 blue) and *Bacillus cereus* (ATCC 10987), were grown to mid-log in Luria (37 °C) or tryptic soy broth (30 °C), respectively, before harvesting by centrifugation at 1200 ×*g* for 10 min (4 °C). Cell pellets were washed twice with phosphate-buffered saline (PBS), pH 7.4 and resuspended in 1/5 original volume of PBS. Cell numbers (in PBS) were then counted by flow cytometry (Accuri C6). Cell suspensions not used immediately were diluted with an equal volume of 60% glycerol in PBS before storage at −20 °C. Prior to analysis, cells were diluted in PBS to the appropriate concentrations.

A Tecan XSafire microtiter plate reader was used to measure the absorbance and fluorescence of the porphyrin-AMP constructs in the presence and absence of bacterial targets. Absorbance was measured from 360 to 800 nm in steps of 2 nm. Fluorescence emission spectra were collected from 500 to 800 nm (2 nm steps) using 415 nm excitation while fluorescence excitation spectra were collected from 385 to 619 nm (2 nm steps) at 730 nm emission. In both cases, a gain of 160 was applied with 50 flashes at 400 Hz, and an integration time of 20 μs was employed. All experiments were conducted in 15% DMSO in order to ensure a homogeneous solution; porphyrin-AMP constructs have low water solubility due to the hydrophobicity of the porphyrin utilized and inherent solubilities of the AMPs. Cell concentrations ranging from 107 to 103 cells/mL were employed. Indicator concentrations were varied from 12 to 0.1 μM. In all cases, difference spectra were calculated as the point-by-point subtraction of indicator only spectra from spectra collected for the indicator in the presence of the target.

Fluorescence spectra for cell pellets utilized a total initial volume of 765 μL with 8 μM indicator and varying target cell concentrations in an Eppendorf tube (1.5 mL). As above, all experiments were conducted in 15% DMSO. The fluorescence of the initial solution was measured before centrifuging at 7500 rpm for 10 min. Supernatant was then removed (665 μL), and the remaining solution and pellet were mixed thoroughly to resuspend components. The fluorescence of both the resulting supernatant and the resuspended pellet were collected using the microtiter plate protocol described above.

CD experiments were carried out using a Jasco J-815 circular dichroism spectrometer (Jasco Inc., Easton, MD). An estimated peptide concentration of ~10 μM was used for each CD measurement. CD spectra were recorded in phosphate buffer (PB), pH 7.0 in the presence or absence of 25 mM sodium dodecylsulfate (SDS; critical micelle concentration of SDS ~8.0 mM), as indicated. The wavelength scan was completed from 190 to 300 nm in a thermally controlled (20 °C) quartz cell having a 0.5 cm path length. Each CD spectrum was the average of three scans collected at a scan rate of 50 nm/min, using a data pitch of 1 nm, digital integration time (D.I.T) of 8 s, band width of 1 nm, and a scan speed of 50 nm per minute. The background spectra (i.e., PB buffer ±25 mM SDS in the cuvette) were measured first, followed by that of the peptide solution. Subtraction of the background (solution) spectrum from that of the peptide solution yielded the spectrum of the peptide in the absence or presence of SDS.

Obtaining accurate concentrations of certain peptides is difficult, but reliable structural content calculations can be performed without knowing the exact concentrations of peptide by *g*-factor analysis [15]. The dimensionless *g*-factor is independent of path length, concentration, amino acid content, and molecular weight and is calculated when the same sample and cell are used for both CD and absorption measurements. A *g*-factor spectrum is calculated by dividing the differential absorbance of left- and right-handed circularly polarized light (A_l and A_r,

Table 1
Antimicrobial peptide characteristics.

Peptide	Sequence	Structure in solution	Structure on interaction	Ref
Indolicidin	ILPWKWPWWPWRR-NH_2	Unstructured	Extended boat	
Cercropin A-melittin hybrid	KWKLFKKIGIGAVLKVLTTGLPALIS-NH_2	Unstructured or β-sheet	Amphipathic α-helix	[1]
Bactenecin	RLCRIVVIRVCR; cyclized via disulfide bridge	β-structured	Minimal change	[32]
Polymyxin E	Fatty acyl chain-BTBBBLLBBT, B = diaminobutyrate; cyclized via the side chain of B4	Cyclized peptide possessing a fatty acyl tail	Minimal, loss of backbone turns	[20]

respectively) by the absorbance at each wavelength (A):

$$g = \frac{(A_l - A_r)}{A} \quad (1)$$

Data on the g-factor as a function of wavelength obtained from the CD scans were deconvoluted using the SP43 algorithm and analyzed using the CONTIN/LL software package [25] to yield the percentages of secondary structure components (α-helix, β-strand, turns, etc.) based on the region between 190 and 240 nm. The program analyzes the g-factor value at each wavelength and compares them with a library of proteins of known secondary structure in order to estimate the percentages of the various secondary structural components. We calculated the mean and 95% confidence interval (CI) for all of the sets of experimental data collected. Student's unpaired t-test was used to determine whether differences in content were statistically significant.

3. Results and discussion

The goal in generation of porphyrin-modified AMPs is to provide a construct capable of detecting bacterial species, in which the AMP component serves as a target recognition "domain" while the porphyrin component provides a mechanism of signal generation; specifically, the spectrophotometric characteristics of the porphyrin are impacted by structural changes in the antimicrobial peptide upon binding of the target. Direct interaction of a porphyrin with the bacterial target may result in changes to the spectrophotometric characteristics, but these will likely be nonspecific. With this in mind, the interaction of the porphyrin (C_1TPP) with the bacterial targets was first evaluated. No concentration dependent changes in the spectrophotometric characteristics of the porphyrin were noted upon interaction with either *E. coli* or *B. cereus*. An overall quench was noted in the fluorescence emission spectra of the porphyrin in the presence of bacterial cells (Supplemental Material, Fig. S-1); dose dependence was not observed.

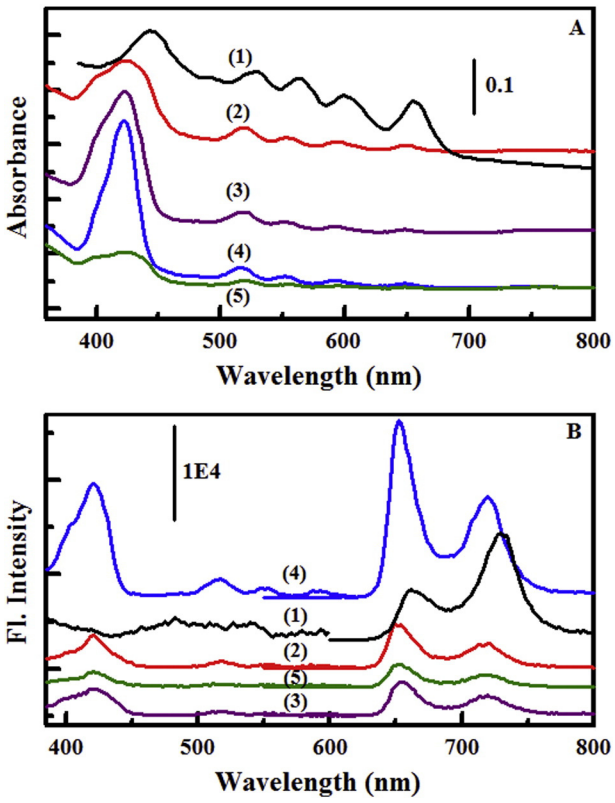

Fig. 1. Porphyrin-modified peptides. Shown here are the absorbance (A) and fluorescence (B) spectra for C_1TPP and the C_1TPP-modified antimicrobial peptides. In absorbance, C_1TPP (1); C_1-Bac (2) shifted +0.25; C_1-Ind (3) shifted +0.1; C_1-CeMe (4); and C_1-PME (5). In fluorescence, C_1TPP (1) shifted +3000; C1-Bac (2); C_1-Ind (3) shifted −5000; C_1-CeMe (4) scaled by 0.5, shifted +7500; and C_1-PME (5) shifted −2000. All compounds in 15% DMSO at 20 μM.

3.1. Porphyrin-AMP constructs

Many, but not all AMPs, undergo a change in structure when interacting with target cells and membranes. In order to evaluate whether binding-mediated changes in an AMP's secondary structures would elicit a corresponding change in porphyrin spectrophotometric properties, we selected four cationic AMPs with different structures and interaction types (Table 1). Specifically, we chose two AMPs whose structures are minimally affected by target binding and two that undergo significant changes in secondary structure upon interacting with cells. The former include bactenecin (Bac), a small β-structured peptide restricted by cyclization [32] and polymyxin E (PME) another cyclized peptide possessing a fatty acyl tail [19]. In both cases, only minor changes in conformation occur upon target binding. On the other hand, both Indolicidin (Ind) and cecropin A-melittin hybrid (CeMe) are extended/unstructured in aqueous solution and undergo significant changes when interacting with target. Ind assumes an extended boat conformation, and CeMe forms an amphipathic α-helix upon binding to target cells and membranes [1]. As shown in Fig. 1, the absorbance characteristics of C_1TPP in solution are distinctly different from those of the C_1TPP-AMP constructs. The varying peak positions in both absorbance and fluorescence as well as differences in extinction coefficients and fluorescence emission tend to indicate unique interactions between the porphyrin and each of the AMPs. It should be noted that the water solubility of the porphyrin alone is low, requiring addition of 15% DMSO to achieve sufficient concentration for collection of spectra. The C_1-Bac and C_1-PME constructs have similar solubility limitations while the C_1-Ind and C_1-CeMe constructs are more soluble.

When incubated in the presence of target bacteria, spectrophotometric changes for the porphyrin-AMP constructs were specific and dependent on the construct considered, the type of bacteria, and the concentrations of the two components. Fig. 2 presents difference spectra for C_1-Ind upon interaction with the two bacterial targets showing a peak/trough pair. While changes in absorbance for the Soret region were noted at similar peak positions, the concentration dependence of the interaction was different for the two types of bacteria (Fig. 2; Supplemental Material, Fig. S-15). Changes in the absorbance spectrum were of larger intensity for the interaction of C_1-Ind with *E. coli* than those observed for the interaction with *B. cereus*. Changes in the fluorescence of the construct were also noted upon interaction with the targets with both targets yielding similar behavior (Supplemental Material, Fig. S-2).

The interaction of C_1-CeMe with the two bacterial targets produced results that were distinct from those observed for C_1-Ind in both the absorbance and fluorescence spectra. For both bacterial targets, only a trough was observed in the Soret region of the absorbance spectrum, centered at 420 nm (Fig. 3). The changes in fluorescence for the interaction of the two targets with C_1-CeMe were small (in the noise for the excitation spectrum; Supplemental Material, Fig. S-3). Constructs comprised of C_1TPP with Bac or PME – the two peptides offering minimal structural rearrangements upon target binding – showed no significant changes in absorbance at any of the evaluated concentrations (Supplemental Material, Figs. S-4 and S-5). Slight changes in fluorescence were noted for only the highest concentrations of C1-PME (20 μM) and targets (1.6×10^7 cell/mL) used; changes were below the threshold needed for effective evaluation. These changes in spectrophotometric character are may be related to indicator solubility rather than specific interactions.

Several possible scenarios would result in the lack of changes in spectrophotometric characteristics upon exposure of the C_1-PME and C_1-Bac indicators to bacterial targets. (1) Changes in the antimicrobial

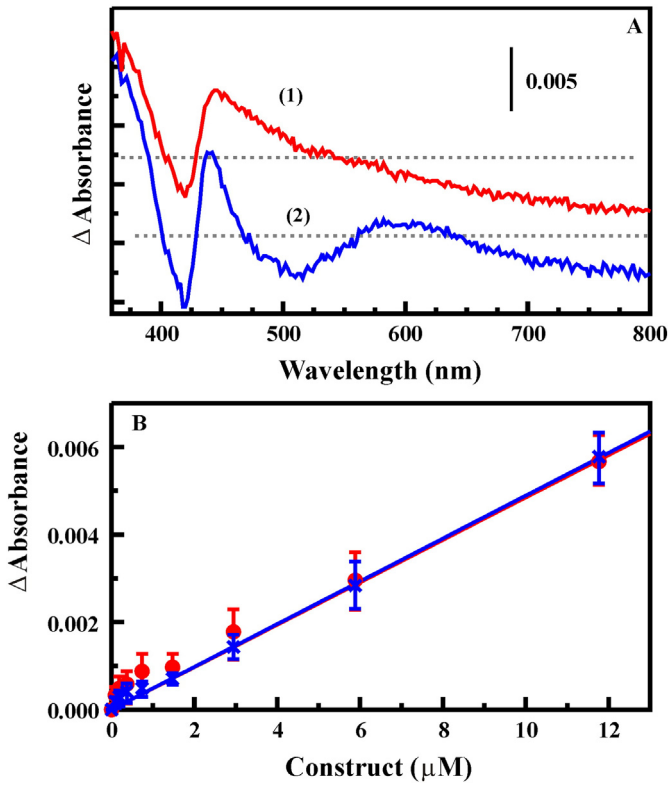

Fig. 2. Interaction of C_1-Ind with bacterial cells. Absorbance difference spectra (A) are calculated as the point-by-point subtraction of the spectrum of the construct alone (20 μM) from that of the construct in the presence of target (i.e., C_1-Ind + *E. coli minus* C_1-Ind): *E. coli* (1; shifted +0.006) and *B. cereus* (2) at 2.4×10^5 cell/mL. Also shown is the concentration dependence (B) of the intensity changes calculated as peak height in the difference spectra (439 nm): *E. coli* (x, 1.9×10^6 cell/mL) and *B. cereus* (circle, 3.8×10^6 cell/mL). Error bars indicate the range of values obtained for replicate measurements.

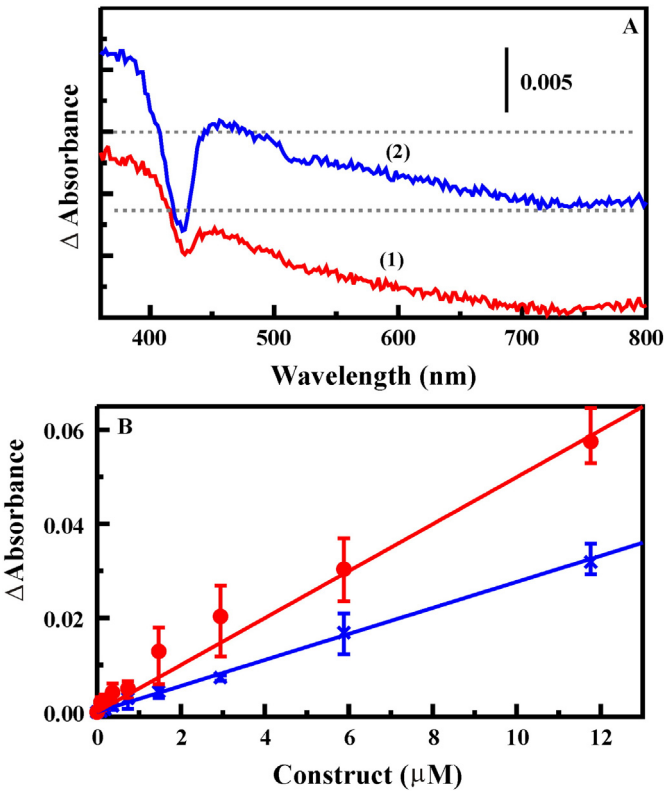

Fig. 3. Interaction of C_1-CeMe with bacterial cells. Absorbance difference spectra (A) are calculated as the point-by-point subtraction of the spectrum of the construct alone (20 μM) from that of the construct in the presence of target (i.e., C_1-CeMe + *E. coli minus* C_1-CeMe): *E. coli* (1) and *B. cereus* (2; shifted −0.006) at 1.6×10^5 cell/mL. Also shown is the concentration dependence (B) of the intensity changes calculated as trough depth in the difference spectra (427 nm): *E. coli* (x, 1.9×10^6 cell/mL) and *B. cereus* (circle, 3.8×10^6 cell/mL). Error bars indicate the range of values obtained for replicate measurements.

peptide upon interaction with the targets could be insufficient to cause a change in the porphyrin environment; this would support our hypothesis that a change in peptide structure upon binding induces a concomitant spectrophotometric change in the porphyrin. (2) The antimicrobial peptides no longer possess characteristics favorable to interaction with the bacteria following porphyrin modification. (3) The affinity of the construct for the target is sufficiently low that changes are not observed across the range of values interrogated. In order to further explore these possibilities, targets and indicators were mixed in microcentrifuge tubes. Fluorescence was evaluated for this initial solution as well as for the pellet and supernatant following centrifugation of the tube. Analysis was completed based on the ratio of the concentration in the pellet to that of the original solution as calculated based on peak fluorescence.

In a tube with no bacterial target, indicator concentrations in pellets containing C_1-Bac were nearly identical to those of the initial solution (ratio = 1.01). The concentration of C_1-Bac in the pellet increased (less indicator in the supernatant) as *B. cereus* concentration increased (Fig. 4); however, no increase in pellet concentrations was noticed in the presence of *E. coli*. C_1-PME showed increasing pellet concentration with increasing target concentration for both *E. coli* and *B. cereus*. There was also significant precipitation of the indicator from solution in the absence of target, likely owing to the more limited solubility of the C_1-PME indicator. Fig. 4 includes data for C_1-Ind and C_1-CeMe for comparison. Based on this analysis, it appears that there are interactions for C_1-PME and C_1-Bac indicators with *B. cereus* and that the C_1-PME indicator interacts with *E. coli*. The lack of interactions between C_1-Bac and *E. coli* would tend to indicate that the AMP structure has been impacted negatively by conjugation with the porphyrin given the fact that native Bac does bind to *E. coli* cells [32]. These types of changes in binding behavior have been reported previously upon conjugation to surfaces [18]. In both cases, when the absorbance and fluorescence spectra of the target containing pellets are compared to normalized indicator only spectra, no significant changes are noted. It is likely that any structural changes occurring upon interaction of the indicators with the bacterial targets are insufficient to cause a change in the spectrophotometric characteristics of the porphyrins.

CD analysis was also used to evaluate changes in the structure of the AMP component of the indicators upon interaction with SDS micelles as representative targets. Porphyrin conjugation, unsurprisingly, lead to significant alteration in the overall secondary structure of the peptides.

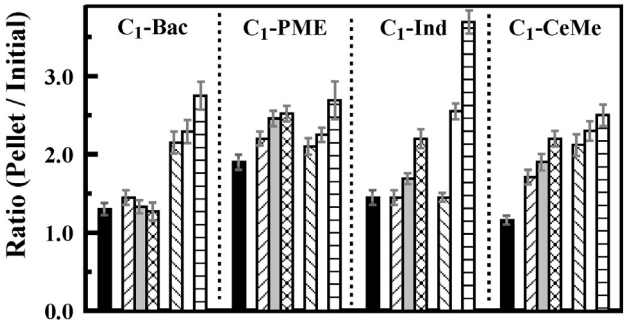

Fig. 4. Pellet analysis. Ratio of peak fluorescence in the pellet following centrifuge to that of the initial target solution. For each indicator, the black bar indicates results in the absence of bacterial cells. The remaining bars are for initial bacteria concentrations (left to right) for *E. coli* at 1.9×10^4, 1.9×10^5, and 1.9×10^6 cell/mL and for *B. cereus* at 2.0×10^4, 2.0×10^5, and 2.0×10^6 cell/mL. Initial construct concentration is 8 μM in all cases.

Significant changes were noted in several structural components of C_1-CeMe and C_1-Ind when exposed to the SDS micelles. This supports the hypothesis that a conformational change in the peptide component of the indicator leads to the observed spectrophotometric changes in the porphyrin component. No significant structural changes were observed for either C_1-Bac or C_1-PME. Quantification of the changes as well as statistical analysis is provided in the Supplemental Material, Figs. S-6 and S-7 and Table S-1.

3.2. Metal complexes

Formation of metalloporphyrin variants strongly impacts both the spectrophotometric characteristics of the porphyrin and its interaction with the environment. It was thought that incorporation of metals into the porphyrin component of the constructs might produce a stronger response to changes in one or more of the constructs. This was of particular interest for the C_1-PME construct where small changes upon target interaction were insufficient for analysis, but indicated the potential for the types of interactions sought under this study. Vanadium, cobalt, and zinc were used to generate metal complexes for the four constructs considered here. Metal incorporation was evaluated based on changes in the fluorescence and absorbance characteristics of the constructs. In all cases, changes in the shape, intensities, and locations of peaks were noted. Fig. 5 presents results for C_1-Ind as an example (additional results in Supplemental Material, Figs. S-8 through S-10). Here, quenching of the fluorescence intensity is noted for the vanadium and cobalt variants, and the zinc construct shows a significant shifts both absorbance and fluorescence. The absorbance spectra show changes in intensity for all of the metal variants with changes in relative intensities across the resulting spectra.

The absorbance and fluorescence characteristics of each of the metal-modified constructs were measured in the presence and absence of varying concentrations of *E. coli* and *B. cereus*. The changes in the spectrophotometric characteristics were distinct for each of the metal complexes of C_1-Ind (Supplemental Material, Fig. S-11). Concentration dependence based on the absorbance spectra indicated that the vanadium version of the construct yielded the largest changes in absorbance (Fig. 5 and Supplemental Material, Fig. S-17) with changes in fluorescence insufficient for analysis (Fig. S-11). The zinc version of the constructed provided significant changes in both absorbance and fluorescence. Given these results, selection of a candidate construct may depend on the application desired, whether utilizing absorbance, fluorescence, or reflectance based interrogation.

Changes in absorbance upon formation of the C_1-CeMe metal complexes were broad and less well defined than those observed for the C_1-Ind construct (Supplemental Material, Fig. S-8). It is possible that incomplete metal complex formation was achieved in this case. Additional incubation time did not result in additional spectrophotometric changes. Based on the data collected, the non-metal C_1-CeMe shows larger changes in both absorbance and fluorescence upon interaction with targets than any of the metal variants (Supplemental Material, Figs. S-12 and S-18). Metal incorporation was evaluated in the PME and Bac (Figs. S-9 and S-10) constructs to assess the possibility that the sensitivity of the porphyrin could be increased leading to changes upon target interaction. This was not the case for these constructs. No significant changes in fluorescence or absorbance were noted for any of the Bac or PME variants (Supplemental Material, Figs. S-13 and S-14).

3.3. Binding affinity

Effective binding affinities for the constructs were determined using an isotherm based on combining the form of the Langmuir isotherm [14] with Beer's Law to obtain a phenomenological model for the

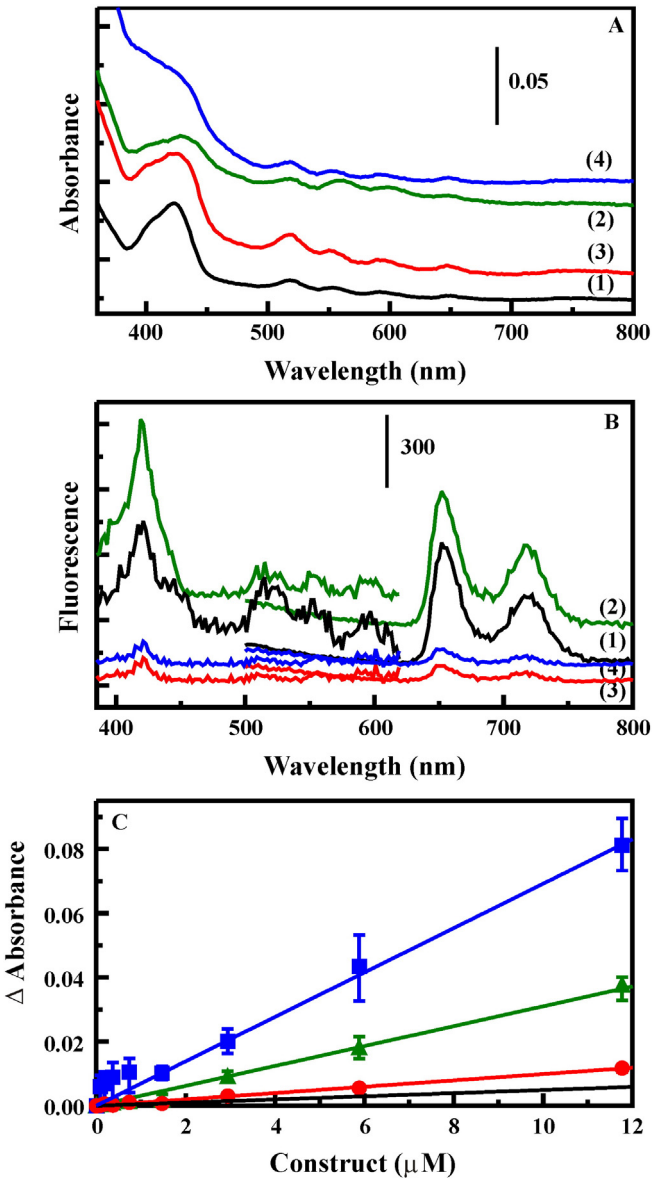

Fig. 5. Metal C_1-Ind constructs. Absorbance (A) and fluorescence (B) spectra for the C_1-Ind variants (8 μM) with vanadium (4), cobalt (3), zinc (2), and no metal (1). Absorbance: VC_1-Ind shifted +0.1 and ZnC_1-Ind shifted +0.085; fluorescence: ZnC_1-Ind shifted +300, VC_1-Ind shifted +50, and C1-Ind shifted +150. Also presented is the concentration dependence (C) for the changes in absorbance upon interaction of these materials with *E. coli* (1.9×10^6 cell/mL): CoC_1-Ind (circle; 422 nm), VC_1-Ind (square; 446 nm), and ZnC_1-Ind (triangle; 428 nm). The fit for C_1-Ind from Fig. 2 is provided for comparison. Complete data sets provided in the Supplemental Material, Fig. S-17.

observed behavior:

$$\Delta A = \Delta\varepsilon \frac{[P_T]k\propto C}{1 + k\propto C} \tag{2}$$

Here, $[P_T]$ yields the typically utilized saturation capacity of the Langmuir model for surface binding. The number of available sites per cell per volume is captured by the variable α, and C is the total cells (refer to the Supplemental Material for additional details on the form of this equation). It is important to note, as with other phenomenological models, the effective affinity coefficient will capture many aspects and features not specifically included in the model, for example, any interdependence of the binding sites. It is also of interest to note that this approach assumes that the cell membrane is not ruptured as a result of the interaction with the construct. Recent models and studies indicate the

Table 2
Binding affinities and spectrophotometric parameters for each of the constructs.

Indicator	Abs (nm)	Ext coeff (M^{-1})	Fl (nm)	Fl coeff (M^{-1}) ($\times 10^7$)	Δε (M^{-1})	ΔF ($\times 10^7$)	kα (M^{-1} L^{-1} mol/cell) ($\times 10^3$)	Δε (M^{-1})	ΔεF ($\times 10^7$)	kα (M^{-1} L^{-1} mol/cell) ($\times 10^3$)
					E. coli			*B. cereus*		
C1-Ind	439	949	650	4.28	519	6.42	103	535	6.80	56.4
ZnC1-Ind	428	9443	650	4.03	3290	1.81	110	3230	1.86	57.4
VC1-Ind	446	11985	–	–	7350	–	102	7150	–	57.8
CoC1-Ind	422	10228	–	–	1050	–	102	1070	–	55.5
C1-CeMe	427	4832	658	13.8	6250	11.8	5.05	6280	10.5	23.3
ZnC1-CeMe	440	3998	660	8.31	2535	–	5.05	–	–	–
VC1-CeMe	435	5734	–	–	5005	–	5.02	–	–	–
CoC1-CeMe	427	3434	–	–	3868	–	5.04	–	–	–

*Fit statistics provided in the supporting information, Table S-2; additional results provided in Table S-3.

need for high concentrations of peptides per cell to achieve rupture [22], and the porphyrin-modified peptides may not be capable of this activity. It is not possible to determine k and α independently on the basis of this equation. While the concentration of bound ligand is not measured directly, ΔA provides the relationship to the bound concentration. Though this expression (Eq. (2)) was derived to describe changes in absorbance, an identical approach can be taken to addressing the fluorescence data. Table 2 provides the parameters obtained from the data sets. Complete data sets used for generation of isotherms are provided in the Supplemental Material, Figs. S-15 through S-18.

If the constructs function as proposed (metallization affects only signal generation by the porphyrin component and not target recognition) the affinities (and total sites, $k\alpha$) between the indicators and bacterial cells, resulting from AMP interaction with a target, should be constant across the metal variants of a given construct. The value of Δε and the associated wavelengths, on the other hand, are expected to vary as they are characteristics of the porphyrin component. As observed for the C_1-Ind construct, the affinity for the four variants is within the error of the fits while the Δε value varies significantly (Table 2). An approximation can be used to related the *ka* values determined here to traditional affinity coefficients by assuming that the number of sites available is ~1.2×10^6 (based on the lipopolysaccharide content of *E. coli* [17]) The calculated value of k for the Ind constructs in this case is on the order of 4.6×10^{12} M^{-1}. This number is higher than that typically reported for the peptide, but the model applied is phenomenological and likely captures features of the system that are not specifically addressed.

Looking at the data from another point of view, if spectrophotometric changes in the constructs result from changes in the AMP structure, as proposed, rather than resulting from direct porphyrin-cell interactions, the Δε value for a construct would be expected to be similar regardless of the type of bacteria evaluated. Affinity, however, could vary between bacterial targets dependent on the properties of the AMP. The number of binding sites available could also vary between cell types. Data sets for both C_1-CeMe and C_1-Ind indicators (Table 2) reflect this behavior. When values for interactions of the indicators with *E. coli* and *B. cereus* are compared, the Δε values vary only slightly.

4. Conclusions

We have demonstrated the potential of porphyrin modified antimicrobial peptides for indication of bacterial targets on the basis of changes in the spectrophotometric characteristics of the construct. Peptides offering little or no change in conformation upon target interaction did not result in constructs that demonstrated changes in absorbance or fluorescence when in the presence of *E. coli* or *B. cereus*. CD analysis confirmed the absence of significant conformational changes in these constructs. Differing spectrophotometric changes were observed with the constructs that did undergo significant conformational changes (C_1-CeMe, C_1-Ind). Formation of metal complexes with the porphyrin component of the construct was shown to alter the spectrophotometric characteristics of the construct as well as the resulting absorbance and fluorescence changes noted upon interaction with a target. Target affinity was not impacted by metallization.

The porphyrin-peptide constructs demonstrated here offer the potential to enable a new type of biosensing approach. Because the construct offers both target recognition and optical transduction, no additional reagents are necessary (e.g., labeled antibody or non-specific dye). The constructs in this study were utilized in solution, but we are currently working to immobilize the porphyrin-peptide constructs. An immobilized array will enable use of these constructs with either fluorescence-based [23] or reflectance-based [9] detectors. In addition, constructs utilizing both alternative peptides and porphyrins are under development. These new materials should offer the potential for development of an array of indicators. As in previously described work, the response of an array of indicators can be utilized to classify the targets detected [11,26], where a single indicator would not provide sufficient information for identification or classification.

Acknowledgments

This research was sponsored by the U.S. Naval Research Laboratory (WU# 69-6595). Participation of E. Archibong was through an ASEE sponsored internship. A. Gleaves and S. Monk were supported through a National Science Foundation (NSF) and Office of Naval Research (ONR) sponsored summer research internship. We have applied the SDC approach ("sequence-determines-credit") for determining the sequence of authors [28]. The views expressed here are those of the authors and do not represent those of the U.S. Navy, the U.S. Department of Defense, or the U.S. Government. The authors declare no competing financial interests.

Appendix A. Supplementary data

Supplementary data to this article can be found online at http://dx.doi.org/10.1016/j.sbsr.2016.02.005.

References

[1] F. Abrunhosa, S. Faria, P. Gomes, I. Tomaz, J.C. Pessoa, D. Andreu, M. Bastos, Interaction and lipid-induced conformation of two cecropin–melittin hybrid peptides depend on peptide and membrane composition, J. Phys. Chem. B 109 (36) (2005) 17311–17319.
[2] L. Baldini, A.J. Wilson, J. Hong, A.D. Hamilton, Pattern-based detection of different proteins using an array of fluorescent protein surface receptors, J. Am. Chem. Soc. 126 (18) (2004) 5656–5657.
[3] L. Bourre, F. Giuntini, I.M. Eggleston, C.A. Mosse, A.J. MacRobert, M. Wilson, Effective photoinactivation of Gram-positive and Gram-negative bacterial strains using an HIV-1 Tat peptide-porphyrin conjugate, Photochem. Photobiol. Sci. 9 (12) (2010) 1613–1620.
[4] R. Dosselli, M. Gobbo, E. Bolognini, S. Campestrini, E. Reddi, Porphyrin–apidaecin conjugate as a new broad spectrum antibacterial agent, ACS Med. Chem. Lett. 1 (2010) 35–38.
[5] R. Dosselli, C. Tampieri, R. Ruiz-González, S. De Munari, X. Ragàs, D. Sánchez-García, M. Agut, S. Nonell, E. Reddi, M. Gobbo, Synthesis, characterization, and photoinduced

antibacterial activity of porphyrin-type photosensitizers conjugated to the antimicrobial peptide apidaecin 1b, J. Med. Chem. (2012).
[6] H.J. Harmon, Specific visible spectral changes induced by guanine binding to cytosine-derivatized porphyrin, J. Porphyrins Phthalocyanines 6 (2002) 73–77.
[7] T. Hasan, M. Hamblin, N. Soukos, in: USPTO (Ed.), Photosensitizer Conjugates for Pathogen Targeting, The General Hospital Corporation, USA, 2007.
[8] B.J. Johnson, N.E. Anderson, P.T. Charles, A.P. Malanoski, B.J. Melde, M. Nasir, J.R. Deschamps, Porphyrin-embedded silicate materials for detection of hydrocarbon solvents, Sensors 11 (2011) 886–904.
[9] B.J. Johnson, J.S. Erickson, J. Kim, A.P. Malanoski, I.A. Leska, S.M. Monk, D.J. Edwards, T.N. Young, J. Verbarg, C. Bovais, R.D. Russell, D.A. Stenger, Miniaturized reflectance devices for chemical sensing, Meas. Sci. Technol. 25 (9) (2014) 095101.
[10] D. Kuciauskas, J. Kiskis, G. Caputo, V. Gulbinas, Exciton annihilation and energy transfer in self-assembled peptide-porphryin complexes depends on peptide secondary structure, J. Phys. Chem. B 114 (2010) 16029–16035.
[11] N.V. Kulagina, G.P. Anderson, F.S. Ligler, K.M. Shaffer, C.R. Taitt, Antimicrobial peptides: new recognition molecules for detecting botulinum toxins, Sensors 7 (11) (2007) 2808–2824.
[12] N.V. Kulagina, K.M. Shaffer, G.P. Anderson, F.S. Ligler, C.R. Taitt, Antimicrobial peptide-based array for *Escherichia coli* and salmonella screening, Anal. Chim. Acta 575 (1) (2006) 9–15.
[13] F. Liu, A. Ni, Y. Lim, H. Mohanram, S. Bhattacharjya, B. Xing, Lipopolysaccharide neutralizing peptide-porphyrin conjugates for effective photoinactivation and intracellular imaging of Gram-negative bacteria strains, Bioconjug. Chem. 23 (2012) 1639–1647.
[14] J.C. Matthews, Fundamentals of Receptor, Enzyme, and Transport Kinetics, CRC Press, Boca Raton, FL USA, 1993.
[15] P. McPhie, Circular dichroism studies on proteins in films and in solution: estimation of secondary structure by g-factor analysis, Anal. Biochem. 293 (1) (2001) 109–119.
[16] M.M. Ngundi, N.V. Kulagina, G.P. Anderson, C.R. Taitt, Nonantibody-based recognition: alternative molecules for detection of pathogens, Expert Rev. Proteomics 3 (5) (2006) 511–524.
[17] H. Nikaido, Multidurg efflux pumps of Gram-negative bacteria, J. Bacteriol. 178 (20) (1996) 5853–5859.
[18] S.H. North, J. Wojciechowski, V. Chu, C.R. Taitt, Surface immobilization chemistry influences peptide-based detection of lipopolysaccharide and lipoteichoic acid, J. Pept. Sci. 18 (6) (2012) 366–372.
[19] P. Pristovsek, J. Kidric, Solution structure of polymyxins B and E and effect of binding to lipopolysaccharide: an MMR and molecular modeling study, J. Med. Chem. 42 (22) (1999) 4604–4613.
[20] P. Pristovšek, J. Kidrič, Solution structure of polymyxins B and E and effect of binding to lipopolysaccharide: an NMR and molecular modeling study‡, J. Med. Chem. 42 (22) (1999) 4604–4613.
[21] E. Reddi, M. Ceccon, G. LValduga, G. Jori, J. Bommer, F. Elisei, L. Laterini, U. Mazzucato, Photophysical properties and antibacterial activity of meso-substituted cationic porphyrins, Photochem. Photobiol. 75 (2002) 462–470.
[22] D. Roversi, V. Luca, S. Aureli, Y. Park, M.L. Mangoni, L. Stella, How many antimicrobial peptide molecules kill a bacterium? The case of PMAP-23, ACS Chem. Biol. 9 (9) (2014) 2003–2007.
[23] C.A. Rowe-Taitt, J.P. Golden, M.J. Feldstein, J.J. Cras, K.E. Hoffman, F.S. Ligler, Array biosensor for detection of biohazards, Biosens. Bioelectron. 14 (10–11) (2000) 785–794.
[24] M. Sibrian-Vasquez, T. Jensen, M. Vicente, Synthesis, characterization, and metabolic stability of porphyrin-peptide conjugates bearing bifunctional signaling sequences, J. Med. Chem. 51 (2008) 2915–2923.
[25] N. Sreerama, R.W. Woody, Estimation of protein secondary structure from circular dichroism spectra: comparison of CONTIN, SELCON, and CDSSTR methods with an expanded reference set, Anal. Biochem. 287 (2) (2000) 252–260.
[26] C.R. Taitt, S.H. North, N.V. Kulagina, Antimicrobial peptide arrays for detection of inactivated biothreat agents, Methods Mol. Biol. 570 (2009) 233–255.
[27] C.R. Taitt, L.C. Shriver-Lake, M.M. Ngundi, F.S. Ligler, Array biosensor for toxin detection: continued advances, Sensors 8 (12) (2008) 8361–8377.
[28] T. Tscharntke, M.E. Hochberg, T.A. Rand, V.H. Resh, J. Krauss, Author sequence and credit for contributions in multiauthored publications, PLoS Biol. 5 (1) (2007) e18.
[29] L.K. Tsou, R.K. Jain, A.D. Hamilton, Protein surface recognition by porphyrin-based receptors, J. Porphyrins Phthalocyanines 8 (1–3) (2004) 141–147.
[30] B.J. White, H.J. Harmon, Interaction of monosulfonate tetraphenyl porphyrin, a competitive inhibitor, with acetylcholinesterase, Biosens. Bioelectron. 17 (6–7) (2002) 463–469.
[31] B.J. White, H.J. Harmon, Optical solid-state detection of organophosphates using organophosphorus hydrolase, Biosens. Bioelectron. 20 (10) (2005) 1977–1983.
[32] M.H. Wu, R.E.W. Hancock, Interaction of the cyclic antimicrobial cationic peptide bactenecin with the outer and cytoplasmic membrane, J. Biol. Chem. 274 (1) (1999) 29–35.
[33] H.C. Zhou, L. Baldini, J. Hong, A.J. Wilson, A.D. Hamilton, Pattern recognition of proteins based on an array of functionalized porphyrins, J. Am. Chem. Soc. 128 (7) (2006) 2421–2425.

Porphyrin-Modified Antimicrobial Peptide Indicators for Detection of Bacteria

Brandy J. Johnson[1*], Chris R. Taitt[1], Apre Gleaves[2], Stella H. North[3], Anthony P. Malanoski[1], Iwona A. Leska[4], Edikan Archibong[5], Stormie M. Monk[6]

[1]Center for Bio/Molecular Science & Engineering, Naval Research Laboratory, Washington, DC 20375-5348

[2]Chemistry Department, Howard University, Washington, DC 20059; at NRL[1] Summer 2013/2014 through NSF / ONR internship

[3]Latham & Watkins LLP, Washington, DC 20004; formerly at NRL[1]

[4]NOVA Research Incorporated, Alexandria, VA, USA 22308

[5]Department of Chemical and Biomedical Engineering, University of South Florida, Tampa, FL 33620; at NRL[1] Summer 2013 through ASEE internship

[6]Fayetteville State University, Fayetteville, NC, USA 28301; at NRL[1] Summer 2012 through ASEE internship

*Corresponding author: brandy.white@nrl.navy.mil

ph: 202-404-6100 fax: 202-767-9598

This supplemental information contains additional absorbance and fluorescence spectra as well as related difference spectra. Also included is additional information on concentration dependence for interactions of the constructs with targets and results of CD analysis.

Figure S-1. Interaction of C_1TPP with bacteria. Absorbance and fluorescence spectra for the C_1TPP (6 μM) in the presence and absence (black) of bacterial cells ($1.8x10^6$): *E. coli* (red) and *B. cereus* (blue).

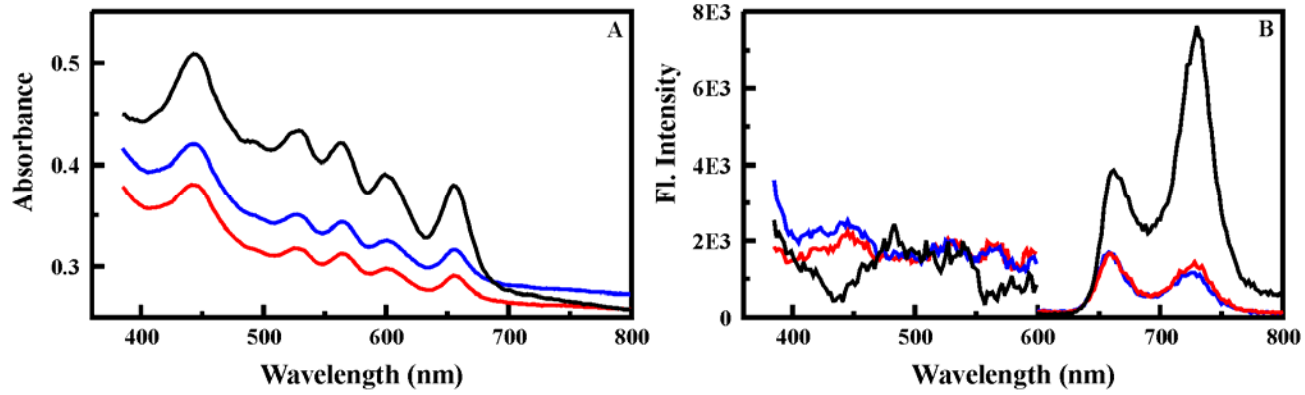

Figure S-2. Interaction of C_1-Ind with bacteria. Fluorescence spectra (A) for C_1-Ind (20 μM) in the presence and absence (black) of bacterial cells ($1.6 x10^6$): *E. coli* (red) and *B. cereus* (blue). Difference spectra are also presented (B).

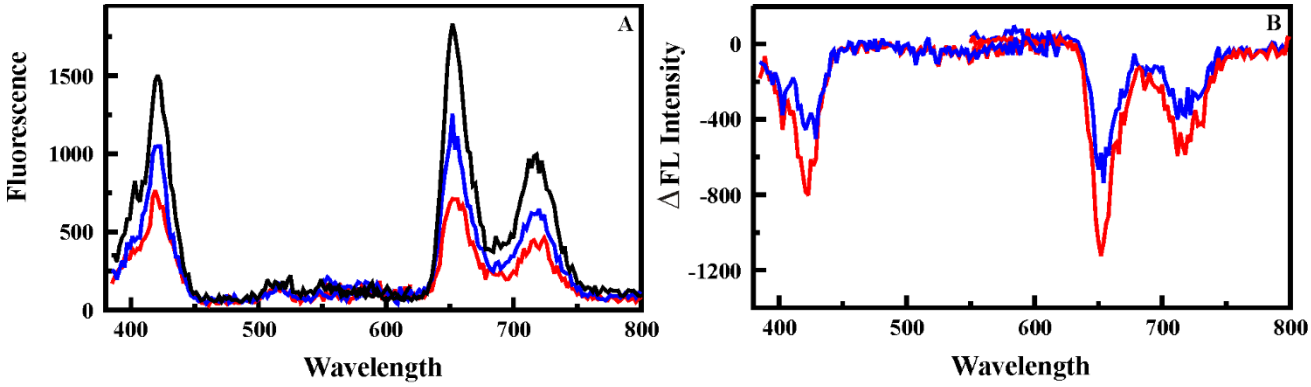

Figure S-3. Interaction of C_1-CeMe with bacteria. Fluorescence spectra (A) for C_1-CeMe (20 μM) in the presence and absence (black) of bacterial cells ($1.8 x10^6$ cell/mL): *E. coli* (red) and *B. cereus* (blue).

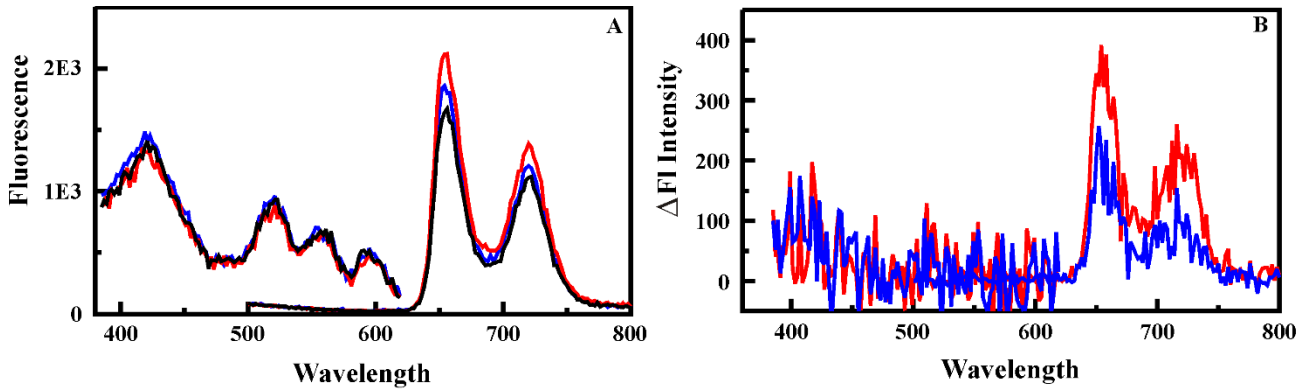

Figure S-4. Interaction of C_1-Bac with bacteria. Absorbance (A) and fluorescence (B) difference spectra for C_1-Bac (11.9 μM) in the presence and absence (black) of bacterial cells (1.9 x10^6 cell/mL): *E. coli* (red) and *B. cereus* (blue).

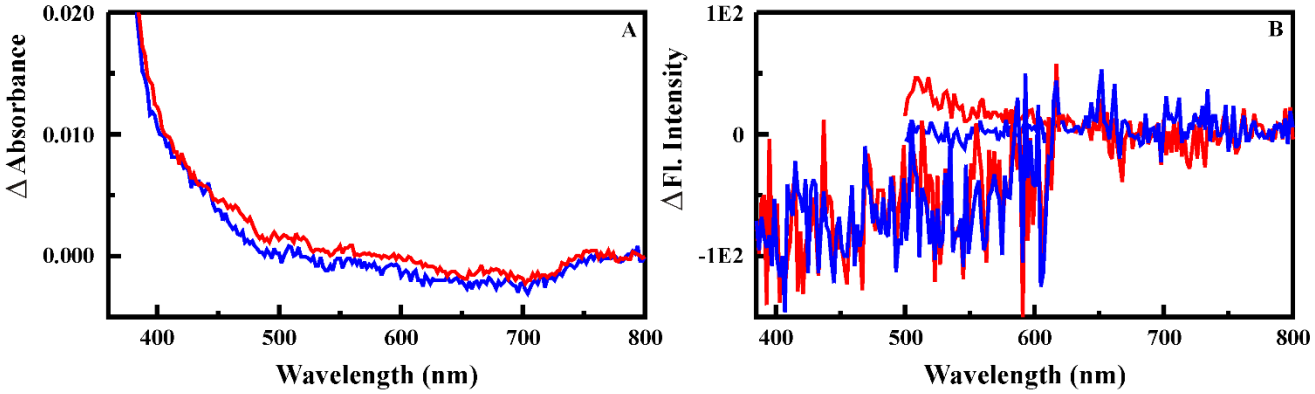

Figure S-5. C_1-PME construct. Absorbance and fluorescence difference spectra for the interaction of C_1-PME (11.9 μM) in the presence and absence (black) of bacterial cells (1.9 x10^6 cell/mL): *E. coli* (red) and *B. cereus* (blue).

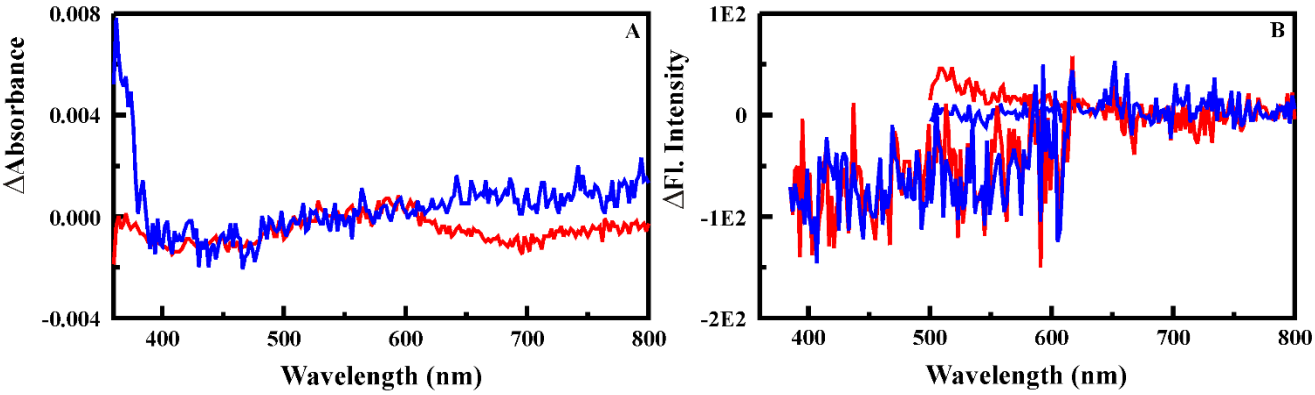

Figure S-6. CD analysis. CD analysis of the peptides and the beacons in the presence (red) / absence (black) of SDS micelles.

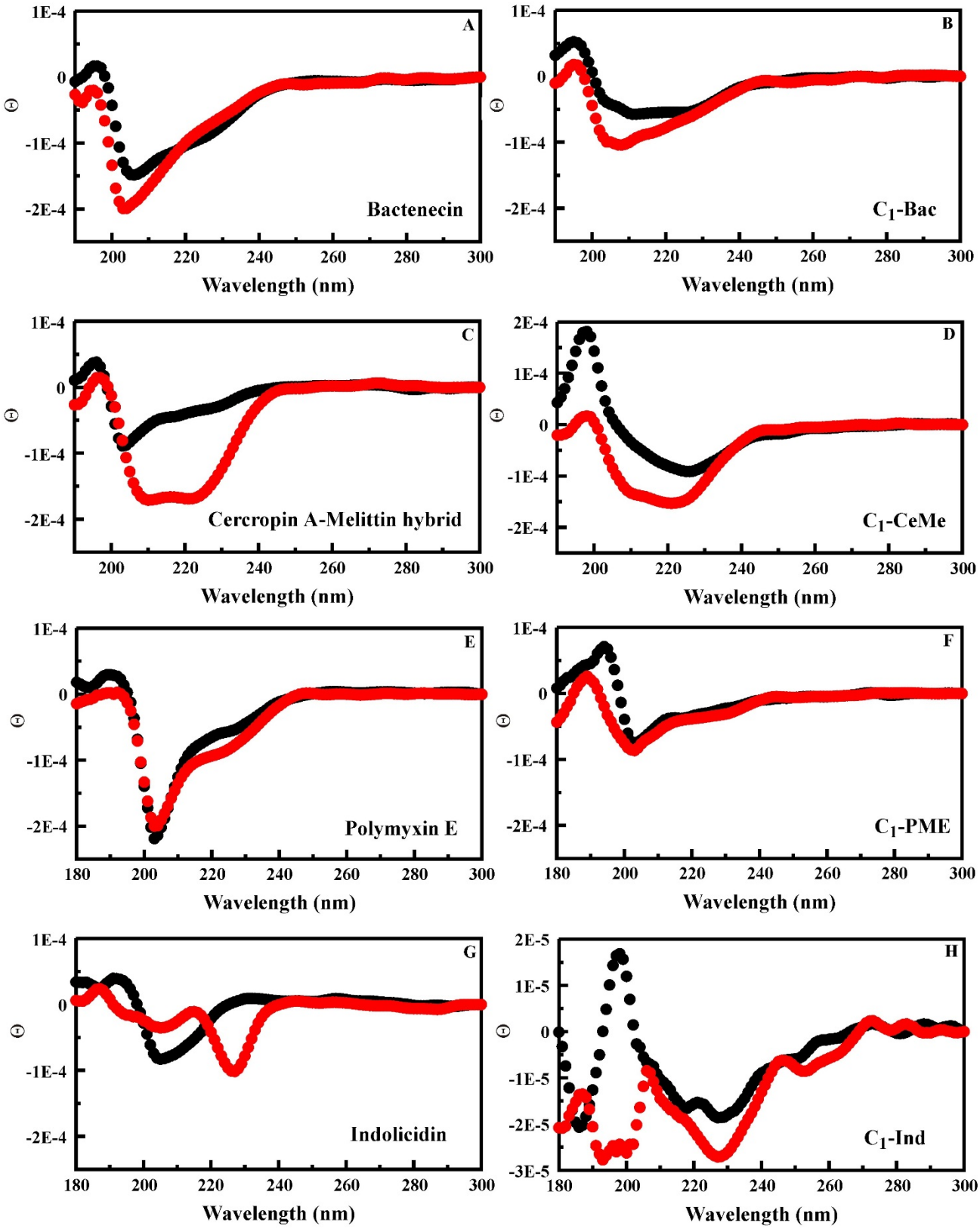

Figure S-7. Structural changes. Shown here are the results of the CD analysis for the beacons in the presence / absence of SDS micelles. Hr: α-helix regular; Hd: α-helix distorted; Sr: β-strand regular; Sd: β-strand distorted; Turn: β-turns; P-values: *significant; **extremely significant

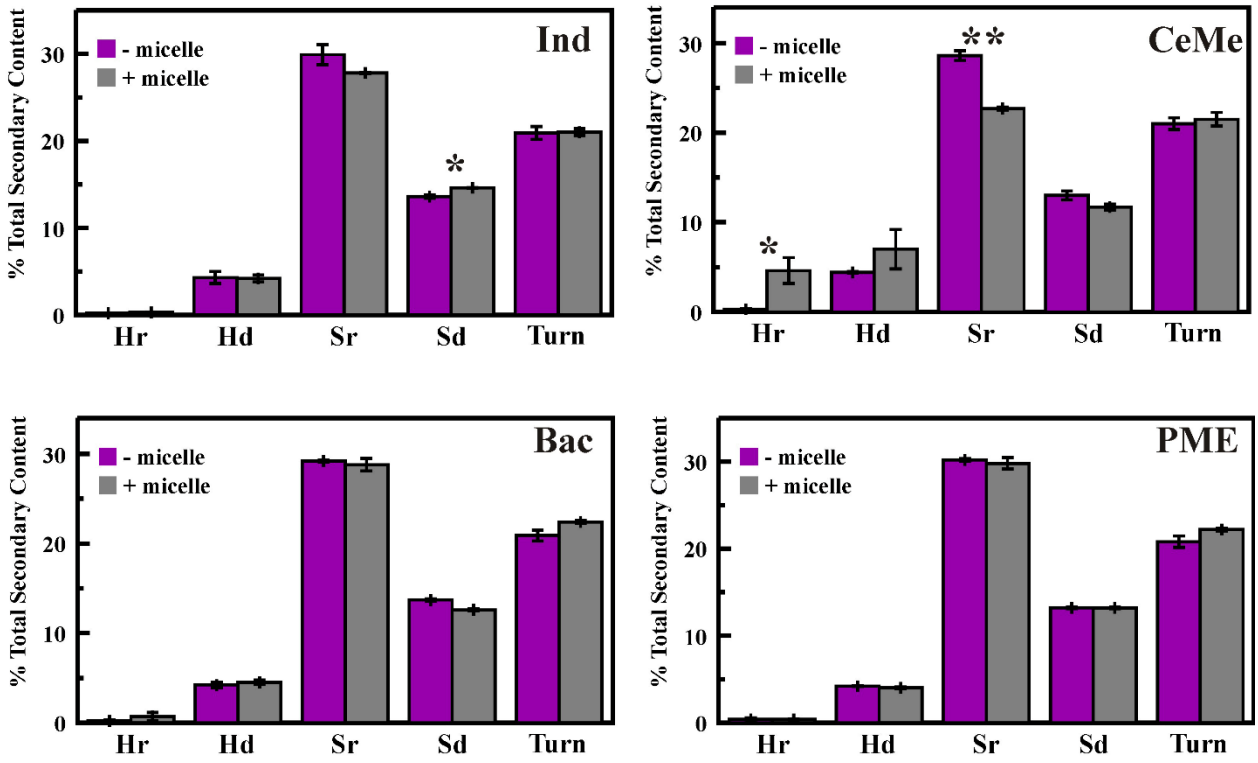

Table S-1. CD analysis for beacons in the presence / absence of SDS micelles showing the average percentage (and standard error) for each type of secondary structure.

Beacon	Micelle	Hr		Hd		Sr		Sd		Turn		Unread	
		Avg	SErr	Avg	SErr	Avg	SErr	Avg	SErr	Avg	SErr	Avg	SErr
C1-Ind	-	0.2	0.00	4.3	0.70	29.9	1.15	13.6	0.20	20.9	0.75	31.3	0.85
	+	0.3	0.05	4.2	0.40	27.8	0.05	14.6	0.05	21.0	0.40	32.4	0.05
C1-CeMe	-	0.3	0.05	4.4	0.10	28.6	0.55	13.0	0.50	21.0	0.65	32.8	0.60
	+	4.6	1.45	7.0	2.20	22.7	0.15	11.7	0.35	21.5	0.75	32.7	2.45
C1-Bac	-	0.2	0.10	4.2	0.30	29.2	0.10	13.7	0.15	20.9	0.60	32.1	0.70
	+	0.7	0.45	4.5	0.25	28.8	0.70	12.6	0.10	22.4	0.15	31.2	0.10
C1-PME	-	0.4	0.15	4.2	0.05	30.2	0.15	13.2	0.10	20.8	0.65	31.4	0.65
	+	0.4	0.05	4.0	0.10	29.8	0.65	13.2	0.10	22.2	0.15	30.6	0.85

Figure S-8. Metal C_1-CeMe constructs. Absorbance and fluorescence spectra for the C_1-CeMe variants (7.8 μM). The spectrophotometric characteristics for the C_1TPP-cercropin A-melittin hybrid construct are presented for the vanadium (blue), cobalt (red), and zinc (green) complexes as well as the original construct (black).

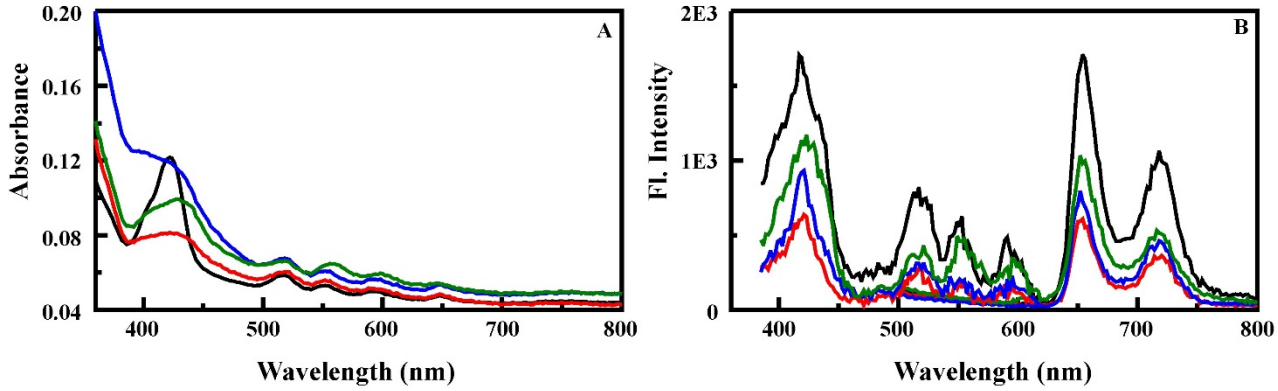

Figure S-9. Metal C_1-Bac constructs. Absorbance and fluorescence spectra for the C_1-Bac variants (7.8 μM). The spectrophotometric characteristics for the C_1TPP-bactenecin construct are presented for the vanadium (blue), cobalt (red), and zinc (green) complexes as well as the original construct (black).

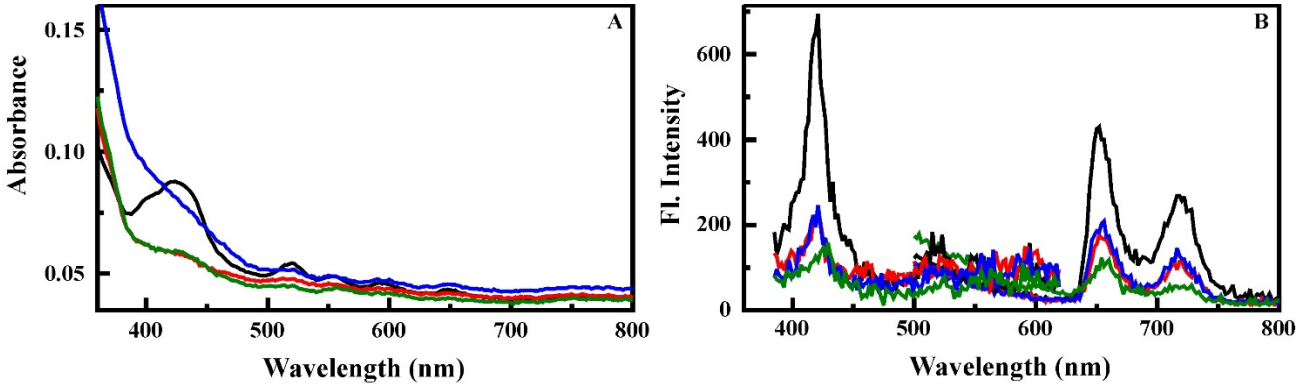

Figure S-10. Metal C_1-PME constructs. Absorbance and fluorescence spectra for the C_1-PME variants (7.8 μM). The spectrophotometric characteristics for the C_1TPP-Polymyxin E construct are presented for the vanadium (blue), cobalt (red), and zinc (green) complexes as well as the original construct (black).

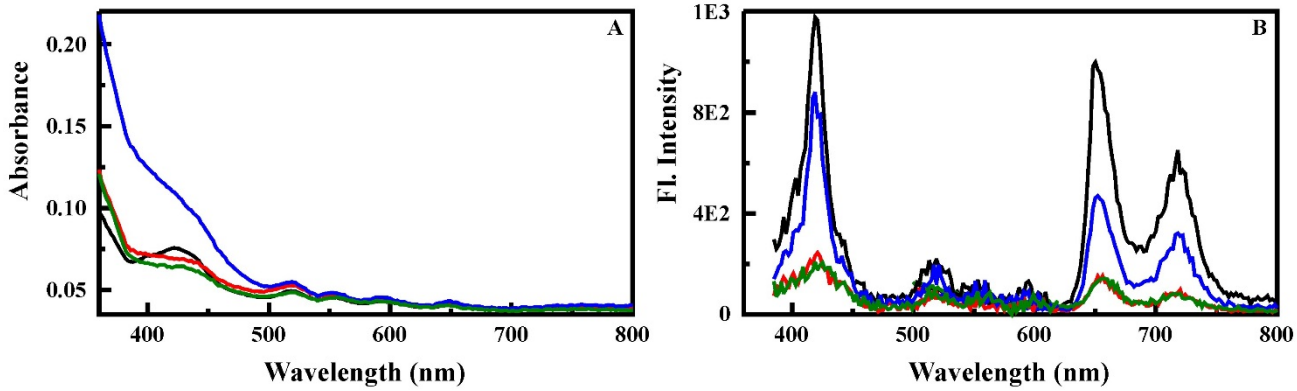

Figure S-11. Metal C_1-Ind constructs. Absorbance and fluorescence difference spectra for the interaction of ZnC_1-Ind (A and B), VC_1-Ind (C and D), and CoC_1-Ind (E and F) (all at 12 μM) with *E. coli* (red; 1.9 x10^6 cell/mL) and *B. cereus* (blue; 2.0 x10^6 cell/mL).

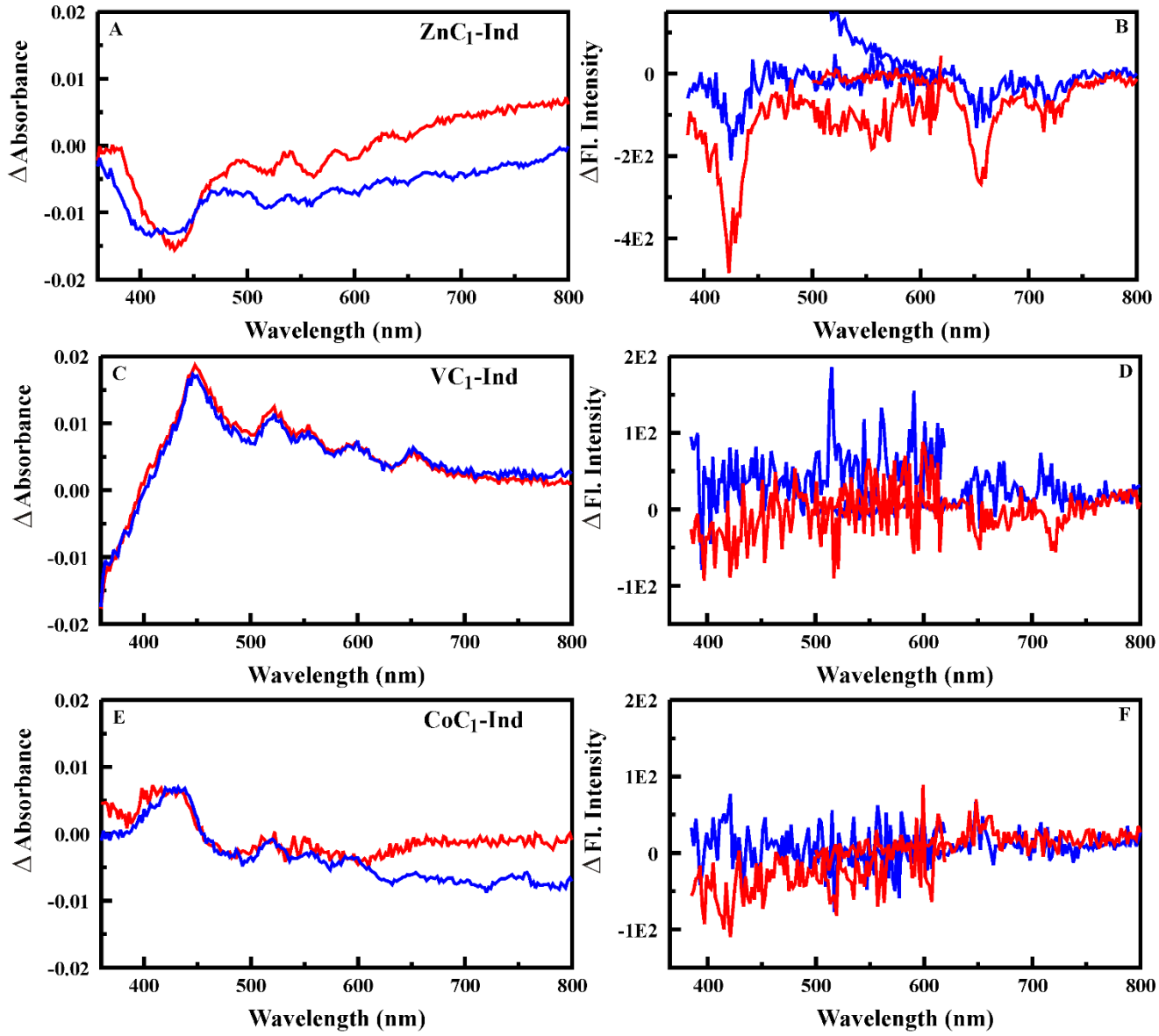

Figure S-12. Metal C_1-CeMe constructs. Absorbance and fluorescence difference spectra for the interaction of ZnC_1-CeMe (A and B), VC_1-CeMe (C and D), and CoC_1-CeMe (E and F) (all at 12 μM) with *E. coli* (red; 1.9 x10^6 cell/mL) and *B. cereus* (blue; 2.0 x10^6 cell/mL).

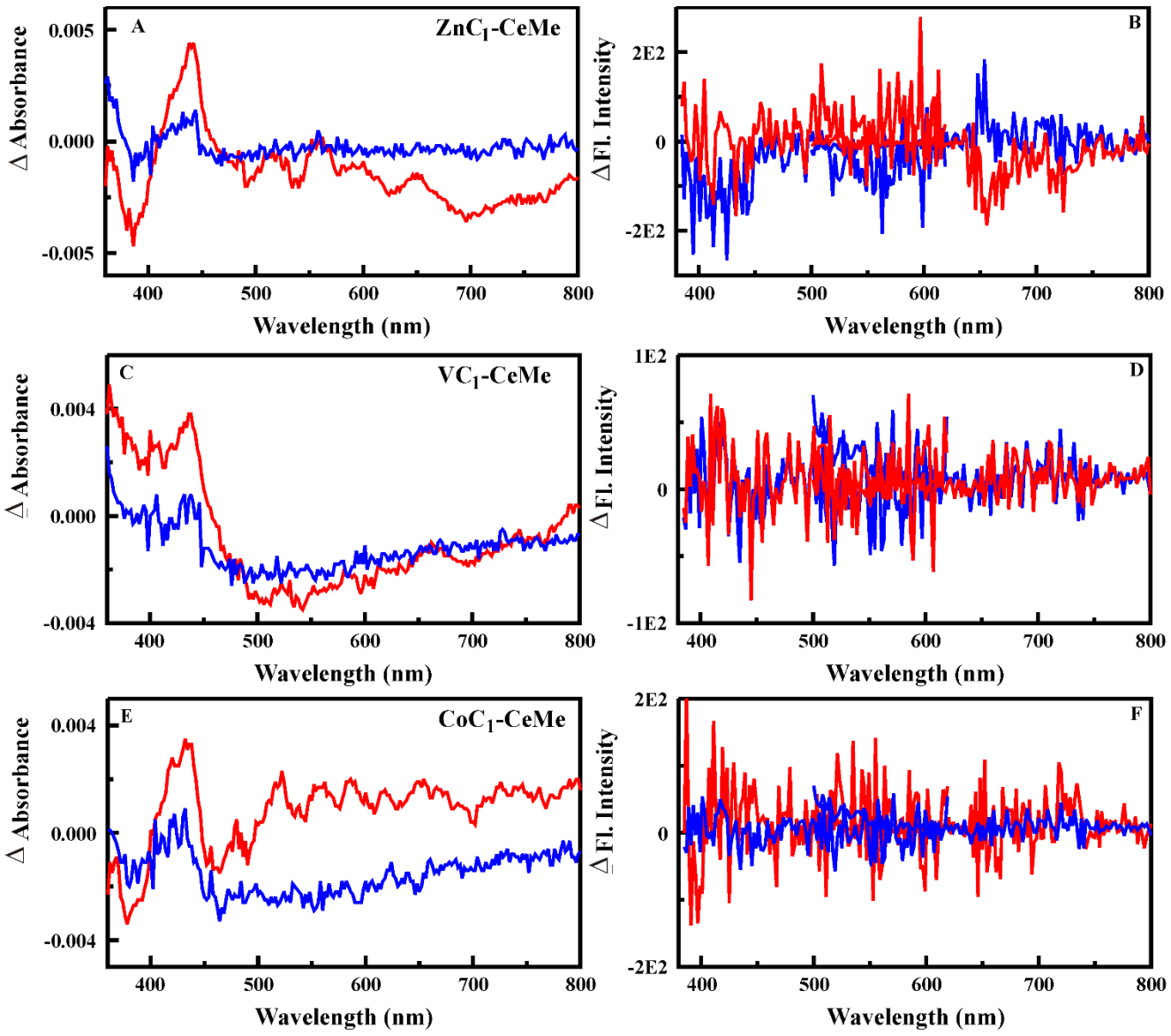

Figure S-13. Metal C_1-Bac constructs. Absorbance and fluorescence difference spectra for the interaction of ZnC_1-Bac (green), VC_1-Bac (blue), and CoC_1-Bac (red) (all at 12 μM) with *E. coli* (A and B; 1.9 x10^6 cell/mL) and *B. cereus* (C and D; 2.0 x10^6 cell/mL).

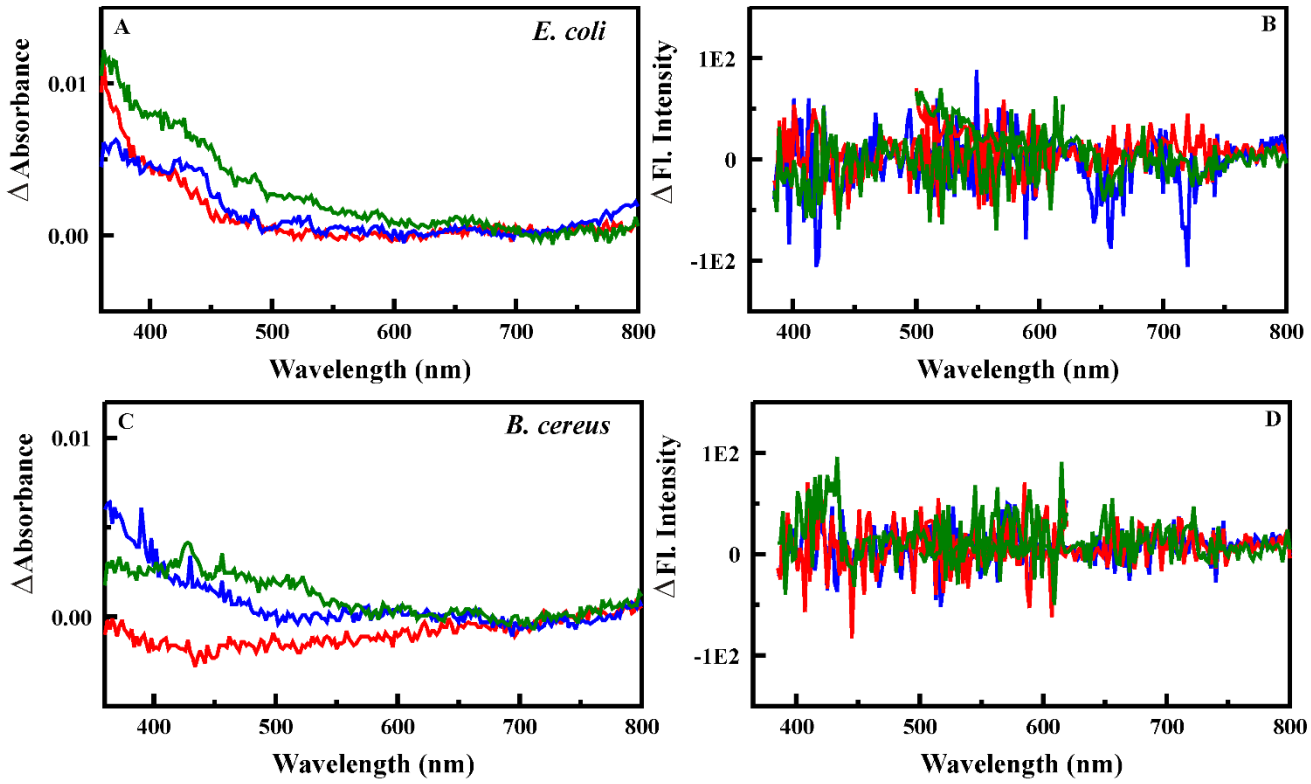

Figure S-14. Metal C_1-PME constructs. Absorbance and fluorescence difference spectra for the interaction of ZnC_1-PME (green), VC_1-PME (blue), and CoC_1-PME (red) (all at 12 μM) with *E. coli* (A and B; 1.9 x10^6 cell/mL) and *B. cereus* (C and D; 2.0 x10^6 cell/mL).

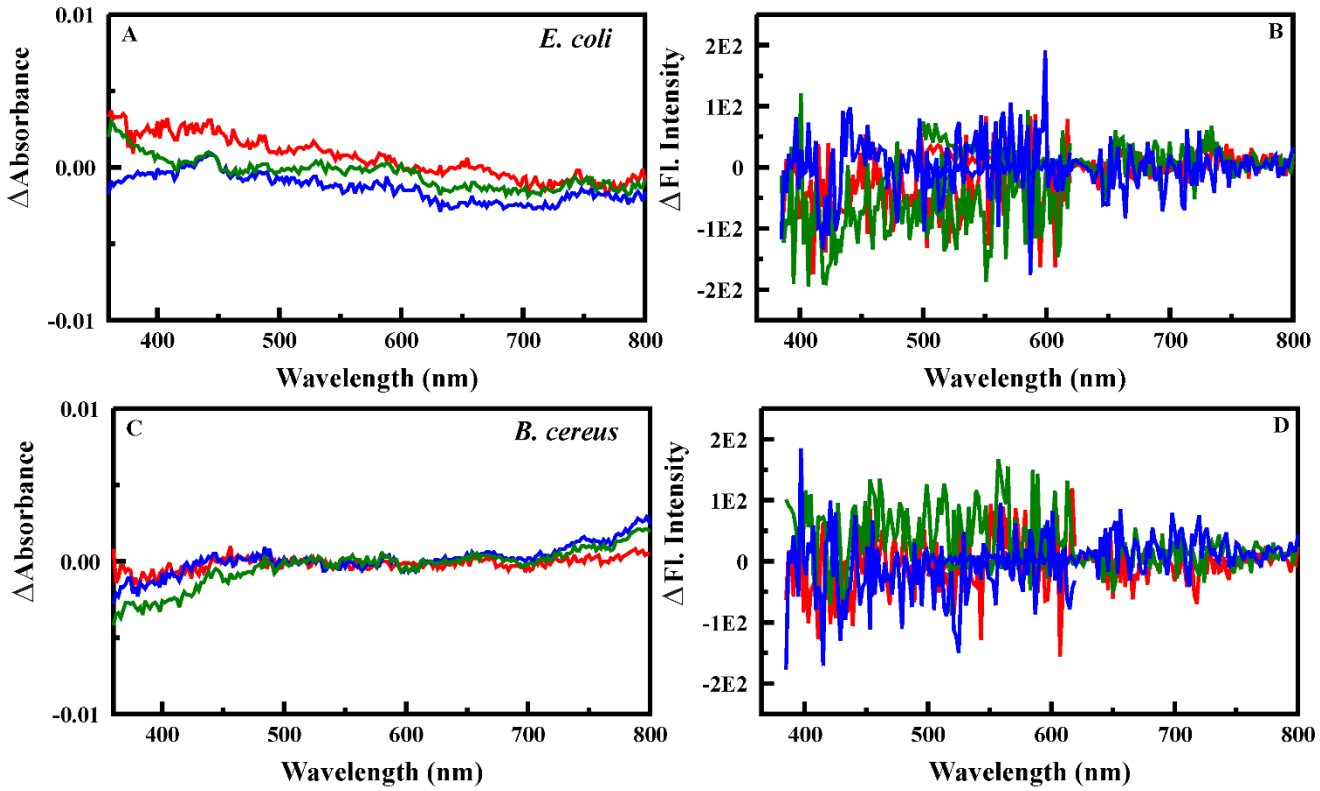

Isotherms.

The absorbance of the system in the absence of target can be represented by Beer's Law:

$$A = \varepsilon b[P_T]$$

where, ε is the extinction coefficient, b is the path length, and $[P_T]$ is the total concentration of the tracer. When target is added, the expression captures the absorbance of the tracer as well as the absorbance of the added target ($\varepsilon_2 C$) and the change in absorbance due to the tracer target complex ($\Delta\varepsilon P_B$):

$$A_C = \varepsilon b[P_T] + \varepsilon_2 b[C] + \Delta\varepsilon b[P_B] \qquad \text{(Eq 1)}$$

The difference absorbance is calculated as post exposure minus pre exposure absorbance:

$$A_C - A = (\varepsilon b[P_T] + \varepsilon_2 b[C] + \Delta\varepsilon b[P_B]) - \varepsilon b[P_T]$$

or

$$\Delta A = \varepsilon_2 b[C] + \Delta\varepsilon b[P_B]$$

In the case of cells at the wavelengths under consideration, $\varepsilon_2 = 0$, reducing the equation to:

$$\Delta A = \Delta\varepsilon[P_B] \qquad \text{(Eq 2)}$$

For simplicity, a path length of one ($b = 1$) is used for the remaining discussion. Assuming a binding isotherm of the form represented by the Langmuir binding isotherm, the tracer bound is:

$$q = \frac{q_s k[L]}{1 + k[L]}$$

where, q_s is the total porphyrin, k is the effective affinity coefficient, and $[L]$ is the concentration of free binding sites; the number of cells x number of sites per cell per volume – αC – if the total tracer occupies a small fraction of the initial sites. Here, $q = [P_B]$:

$$[P_B] = \frac{[P_T]k \propto C}{1 + k \propto C}$$

Relating the measured parameter (ΔA from Eq. 2) to the binding isotherm:

$$\Delta A = \Delta\varepsilon[P_B] = \Delta\varepsilon \frac{[P_T]k\propto C}{1+k\propto C} \qquad \text{(Eq 3)}$$

This is the form of the equation used to generate the parameters (Δε or ΔF and kα) provided in Table 2 and Table S-2.

Table S-2. Fitting statistics for binding affinities and spectrophotometric parameters (provided in Table 2).

Tracer	Absorbance		Fluorescence	
	Chi-Sq	**Std. Err.**	**Chi-Sq**	**Std. Err.**
E. coli				
C1-Ind	9.95e-7	1.99e-4	9090	19.1
ZnC1-Ind	3.08e-6	3.51e-4	3220	11.4
VC1-Ind	2.98e-4	3.45e-3	--	--
CoC1-Ind	6.06e-5	1.56e-3	--	--
C1-CeMe	3.36e-5	1.16e-3	9086	36.8
ZnC1-CeMe	1.77e-5	5.02e-4	--	--
VC1-CeMe	4.65e-5	8.73e-4	--	--
CoC1-CeMe	4.42e-5	8.80e-4	--	--
B. cereus				
C1-Ind	2.87e-6	3.39e-4	4030	14.0
ZnC1-Ind	9.36e-6	3.44e-4	4490	7.54
VC1-Ind	5.61e-4	2.67e-3	--	--
CoC1-Ind	6.06e-5	1.65e-3	--	--
C1-CeMe	8.05e-4	3.18e-3	9075	46.2

Table S-3. Additional spectrophotometric parameters. Fluorescence excitation collected at 730 nm emission; fluorescence emission collected at 415 nm excitation.

Tracer	Absorbance wavelength (nm)[1]	Extinction coefficient (M^{-1})	Fluorescence Wavelength (nm) [1]	Fluorescence Coefficient (M^{-1})	Fluorescence Wavelength (nm)[1]	Fluorescence Coefficient (M^{-1})
C1TPP	443	605	650	6.26e6	730[2]	2.69e7
C1-Ind	439	949	650	4.28e7	419	6.38e7
ZnC1-Ind	428	9443	650	4.03e7	419	5.04e7
VC1-Ind	446	11990	650	1.40e7	419	7.36e7
CoC1-Ind	422	10230	650	1.34e7	419	6.38e7
C1-CeMe	427	4832	658	1.38e8	736[2]	5.05e7
ZnC1-CeMe	440	9700	660	7.65e7	423	9.80e7
VC1-CeMe	435	11870	650	5.76e7	417	7.58e7
CoC1-CeMe	427	8544	650	4.99e7	419	5.37e7
C1-Bac	420	9305	650	9.21e7	421	1.07e8
ZnC1-Bac	424	7354	650	1.40e7	419	1.90e7
VC1-Bac	424	10920	650	3.71e7	419	6.68e7
CoC1-Bac	430	7440	650	1.34e7	419	2.26e7
C1-PME	428	7540	650	3.96e7	419	5.97e7
ZnC1-PME	428	6858	650	9.88e6	419	1.18e7
VC1-PME	428	8626	650	1.71e7	419	1.72e7
CoC1-PME	428	6664	650	1.42e7	419	1.74e7

[1]Peak absorbance / fluorescence from Soret region used for tracers where no changes upon cell interaction are observed.

[2] Value from emission spectrum rather than excitation due to lack of fluorescence observed across the collected excitation spectrum.

Figure S-15. C_1-Ind binding isotherms. Full data sets for the interaction of C_1-Ind with *E. coli* and *B. cereus* at varied cell and tracer concentrations. (A) Absorbance changes for *E. coli* interaction, 432 nm. (B) Fluorescence change for *E. coli* interaction, 650 nm. (C) Absorbance change for *B. cereus* interaction, 432 nm. (D) Fluorescence change for *B. cereus* interaction, 650 nm. Lines indicate the fit contour generated for the cell concentration of the matching color. Fit parameters provided in Table 2.

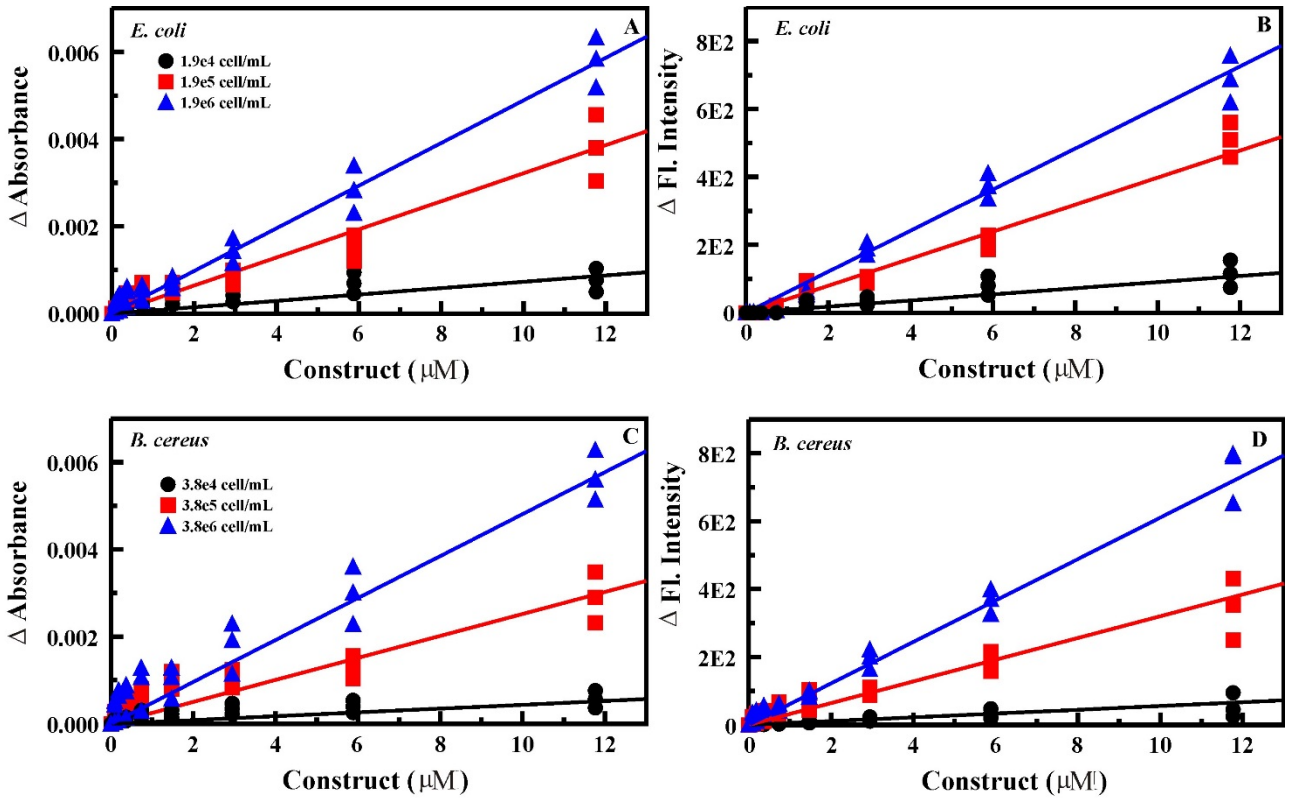

Figure S-16. C_1-CeMe binding isotherms. Full data sets for the interaction of C_1-CeMe with *E. coli* and *B. cereus* at varied cell and tracer concentrations. (A) Absorbance changes for *E. coli* interaction, 427 nm. (B) Fluorescence change for *E. coli* interaction, 658 nm. (C) Absorbance change for *B. cereus* interaction, 427 nm. (D) Fluorescence change for *B. cereus* interaction, 658 nm. Lines indicate the fit contour generated for the cell concentration of the matching color. Where full contours are not included (green circles), x marks the calculated value from the fit. Fit parameters provided in Table 2.

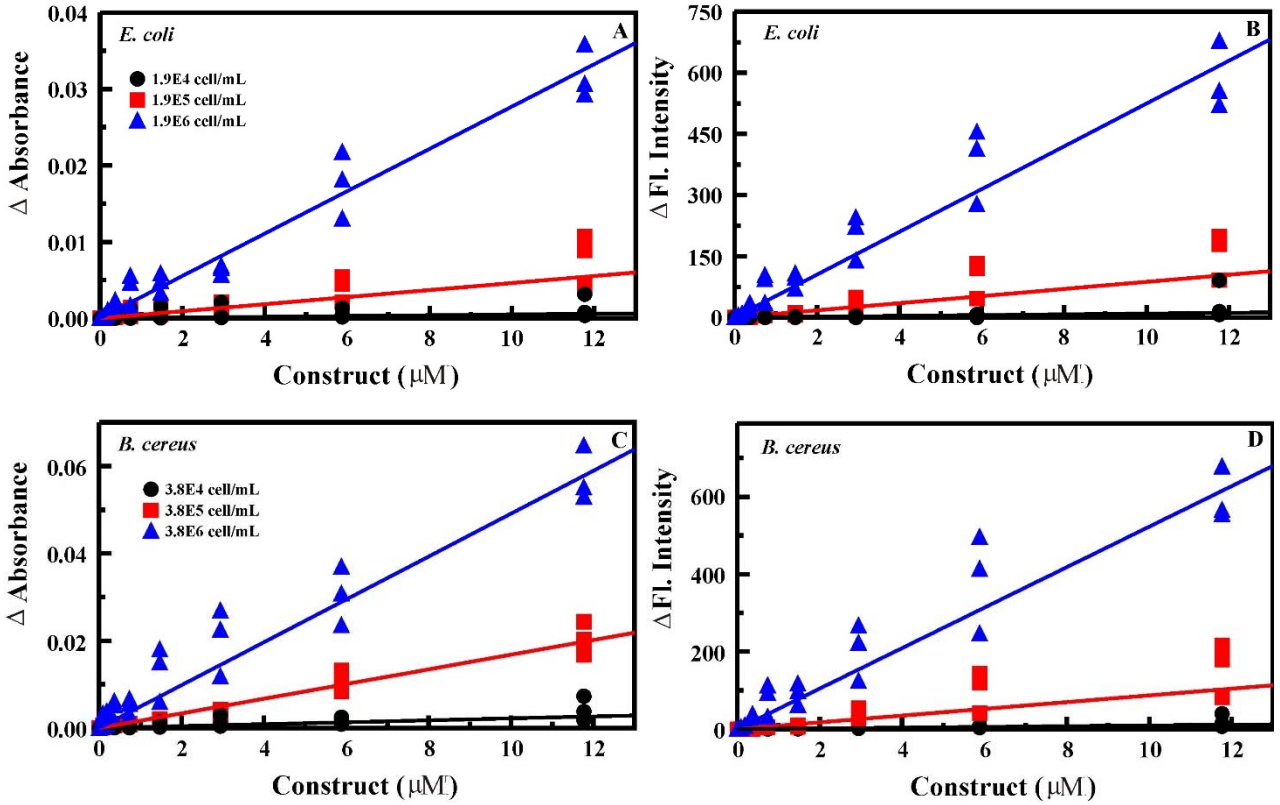

Figure S-17. Metal C_1-Ind binding isotherms. Full data sets for the interaction of the metal C_1-Ind variants with *E. coli* and *B. cereus* at varied cell and tracer concentrations. (A) Absorbance changes for interaction of ZnC1-Ind with *E. coli*, 428 nm. (B) Fluorescence changes for interaction of ZnC1-Ind with *E. coli*, 650 nm. (C) Absorbance changes for interaction of ZnC1-Ind with *B. cereus*, 428 nm. (D) Fluorescence changes for interaction of ZnC1-Ind with *B. cereus*, 650 nm. (E) Absorbance changes for interaction of CoC1-Ind with *E. coli*, 422 nm. (F) Absorbance changes for interaction of CoC1-Ind with *B. cereus*, 422 nm. (G) Absorbance changes for interaction of VC1-Ind with *E. coli*, 446 nm. (H) Absorbance changes for interaction of VC1-Ind with *B. cereus*, 446 nm. Lines indicate the fit contour generated for the cell concentration of the matching color. Fit parameters provided in Table 2.

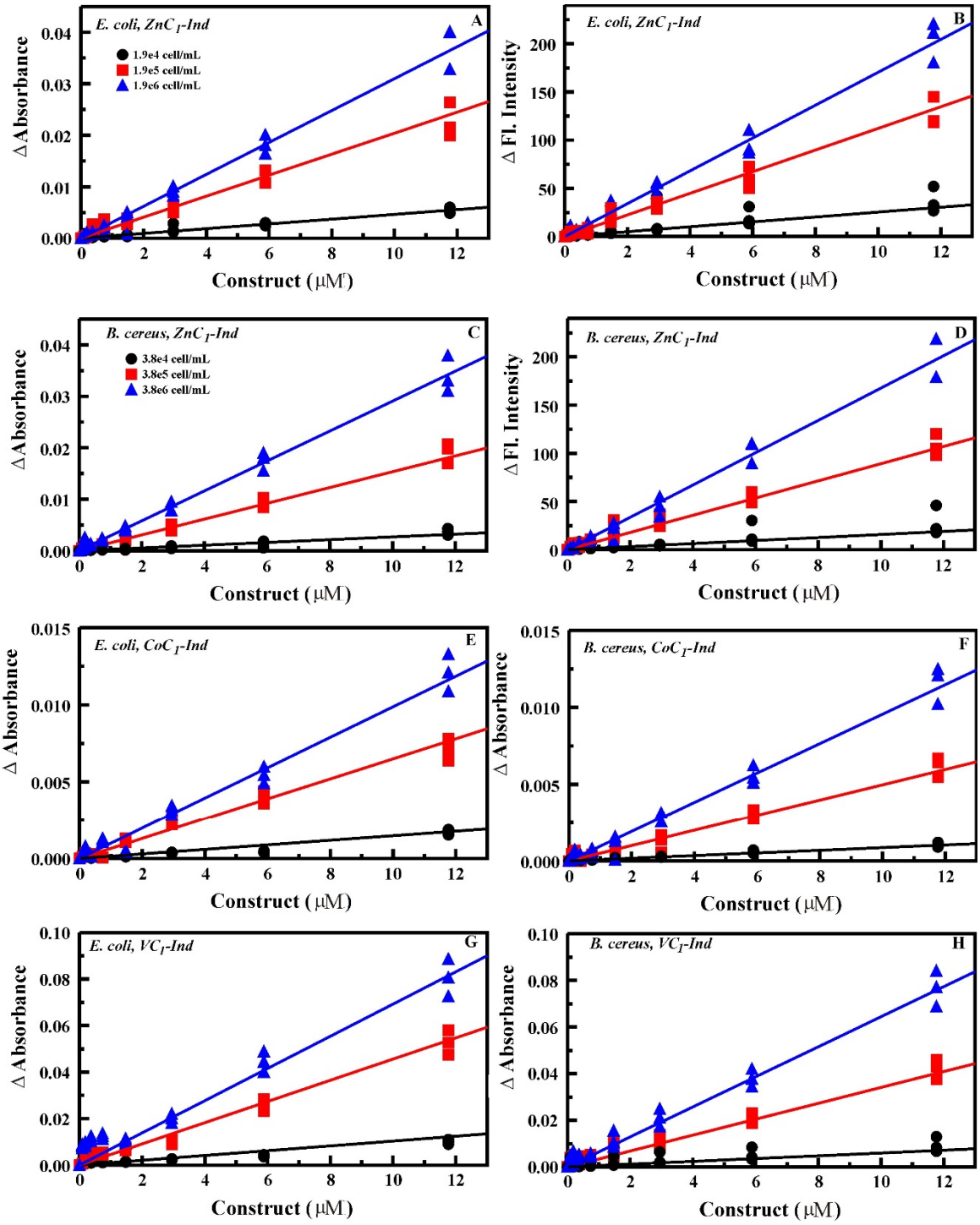

Figure S-18. Metal C_1-CeMe binding isotherms. Full data sets for the interaction of the metal C_1-CeMe variants with *E. coli* at varied cell and tracer concentrations. (A) Absorbance changes for interaction of CoC1-CeMe with *E. coli*, 427 nm. (B) Absorbance changes for interaction of VC1-CeMe with *E. coli*, 435 nm. (C) Absorbance changes for interaction of ZnC1-CeMe with *E. coli*, 440 nm. (D) Fluorescence changes for interaction of ZnC1-CeMe with *E. coli*, 660 nm. Lines indicate the fit contour generated for the cell concentration of the matching color. Fit parameters provided in Table 2.